Cluster observations of hot He^+ events in the inner magnetosphere

M. Yamauchi[1], I. Dandouras[2,3], H. Rème[2,3], and H. Nilsson[1]

1. Swedish Institute of Space Physics, P.O. Box 812, 98128 Kiruna, Sweden
2. CNRS, Institut de Recherche en Astrophysique et Planetologie (IRAP), BP 44346, 31028, Toulouse cedex 4, France
3. University of Toulouse, UPS-OMP, IRAP, Toulouse, France

Abstract

In the inner magnetosphere inside 65 degree invariant latitude, Cluster Ion Spectrometry (CIS) detected hot He^+ events of about a few tens to several hundred eV without the same types of hot H^+ signature at the same energy. During the 2001–2006 period when the Cluster orbit was almost constant and approximately north–south symmetric at constant local time near the perigee, we found nearly 20 examples in Cluster spacecraft 4. These hot He^+ events are morphologically classified into two burst types and two dispersed types:

1. Short intensification of He^+ (1a) without corresponding H^+ or O^+ signatures, or (1b) with H^+ signature at different pitch angles.
2. Energy-latitude dispersed He^+ stripes that continues for tens of minutes at hundreds to a few thousand eV range (2a) at different drift shell from energy-latitude dispersed H^+ stripes, or (2b) with very weak H^+ signature if the energy is constant.

While type-1a is observed during or right after substorm activities, type-2b is found after long quiet periods, i.e., after long drift. The relationship with the geomagnetic activity indicates that the plasmasphere can be energized in a mass dependent way in the evening sector during substorms to form the bursty types (type-1), while the selective He^+ energization can also take place during quiet periods near the noon. On the other hand, the source of the two dispersed types (type-2) must be remote from the observation point, and the location and the geomagnetic conditions at the time of the He^+ filtering is an open question.

(accepted manuscript)
J. Geophys. Res., 119(4), 2706-2716, 2014 (© 2014 by the American Geophysical Union)
https://doi.org/10.1002/2013JA019724

(published 14 April 2014)

citation: Yamauchi, M., Dandouras, I., Rème, H., and Nilsson, H. (2014): Cluster observations of hot He+ events in the inner magnetosphere, J. Geophys. Res. Space Physics, 119(4), 2706-2716, doi:10.1002/2013JA019724.

1. Introduction

The inner magnetosphere inside the geosynchronous orbit (hereafter we consider only this limited region of the inner magnetosphere) shows large variations in both dynamics and ion distributions although the region is separated from the solar wind injection or substorm onset region [e.g., Blanc et al., 1999, and references therein]. The majority of these dynamics and ion populations are ultimately driven or supplied by external phenomena such as substorms, ionospheric outflow, solar wind disturbances, or interplanetary coronal mass ejections. However, the inner magnetosphere has also active roles in energization and ion filtering. One important step toward understanding the own roles of the inner magnetosphere is to separate the externally supplied population and the internal population. For example, in the inner magnetosphere, the low energy ions (sub hundred-eV) normally indicate ionospheric ion, and the hot or energetic ions (more than a hundred eV) are thus normally indicate energization in the magnetosphere.

In this respect, single-charged helium ion (He^+) is a unique species because of its abundance in the plasmasphere, a part of the inner magnetosphere with cold ion dominance. In fact He^+ has been used as a maker of plasmaspheric ions in the magnetosphere [e.g., Williams et al., 1992; Sandel et al., 2000; Yoshikawa et al., 2000; Burch et al., 2001; Dandouras et al., 2005, Darrouzet et al., 2009a,b, and references therein]. Using the fact that the He^+ outside the Earth's shadow resonantly scatters the solar 30.4 nm radiation, the Extreme Ultraviolet Imager (EUV) onboard the IMAGE spacecraft has imaged the distribution of the He^+ ion in the Earth's plasmasphere that glows at 30.4 nm emission [Sandel et al., 2000, 2003]. Although the source of He^+ can be both the plasmasphere and the ionosphere (the plasmaspheric He^+ might originally come from the latter), the He^+/O^+ ratio is normally higher in the plasmasphere than in the topside ionosphere or ring current [e.g., Blanc et al., 1999, and references therein]. Since the plasmaspheric ions are very cold (less than 10 eV), the location and energy of magnetospheric He^+ can be and have been used in understanding the transport and energization of the plasmaspheric ions in the inner magnetosphere [Nakamura et al., 2000; Burch, 2005; Dandouras, 2013].

Within the inner magnetosphere, cold He^+ ions are normally observed simultaneously with protons (H^+) because the plasmasphere normally contains more H^+ than He^+, except in the O^+ plasma trough during the recovery phase of magnetic storms determined by the Dst index [Denton et al., 2002], when the He^+ density approaches the depleted O^+ density that still exceeds the H^+ density at the topside of the ionosphere. This makes the hot He^+ (we call the 30 eV to 3 keV range "hot" in this paper) a minor species with respect to H^+ or O^+ for given energy and pitch angles [Geiss et al., 1979; Young et al., 1982; Lennartsson and Sharp, 1982; Collin et al., 1988; Fuselier and Anderson, 1996; Mouikis et al., 2002; Peterson et al., 2008].

This is consistent with the three main energization mechanisms that are proposed for the hot He^+ in the inner magnetosphere: (1) the field-aligned potential drops (that are important for ion escape from the ionosphere) predict the same pitch angles and energies for He^+ as for H^+ and O^+ at the same location, unless the velocity filter effect for potential acceleration changes the destination significantly [Collin et al., 1988; Peterson et al., 2008]; (2) the ion drift theory predicts the same drift velocity for different species if the energy and the pitch angle are the same [Alfvén and Fälthammer, 1963, chapter 2; Roederer, 1970, chapter 2] even after

adiabatic energization [Ejiri et al., 1980]. (3) The ion energization by the electrostatic ion cyclotron waves [Young et al., 1981, 1982; Fuselier and Anderson, 1996; Horne and Thorne, 1997; Mouikis et al., 2002; Peterson et al., 2008] works for both H^+ and He^+ if the wave is not generated by the H^+ population. Therefore, it is surprising if hot He^+ is observed as the primary ion species among three species (H^+, He^+ and O^+) for given pitch-angles and energies.

Meanwhile, there are observational indications that He^+ might be accelerated to different energies than H^+ or O^+. Johnson et al. [1974] and Lund et al. [1998] showed cases where He^+ is the major component in the precipitating ions to the ionosphere. Peterson et al. [2008] statistically showed that the average characteristic energy of He^+ is not exactly the same as those of O^+ and H^+. It is important to investigate what causes the He^+ distribution different from those of H^+ and O^+ in a systematic case search. This is the main objective of the present work because no systematic examination of differences between the He^+ behavior and the H^+ behavior has been performed so far.

With four spacecraft and a high inclination, Cluster [Escoubet et al., 1997, 2001] is one of the most ideal satellite projects to study the He^+–H^+ differences in the inner magnetosphere at around 4–7 Earth radii (R_E). Surprisingly, the Cluster Ion Spectrometry (CIS) COmposition DIstribution Function (CODIF) instrument [Rème et al., 2001] occasionally observed hot He^+ (peak differential energy flux at 50–500 eV) without, or with a very weak, H^+ signatures. These hot He^+ are not charge-exchanged He^{++} [e.g., Roeder et al., 1996] because the He^{++} counting rate was very low during these He^+ events. The absence of hot He^{++} during the presence of He^+ has been statistically shown by Young et al. [1982] using GOES data, and we can ignore the charge exchange scenario in this region.

We also found examples where the space-time location of associated He^+ and H^+ are different to each other. These appearances of He^+ are not due to the high background convection velocity under strong electric field, as observed by Yamauchi et al. [2009a]. We report CIS/CODIF observations of these unusual events (a total of about 20-30 events during 2001-2006) in this paper. Here, we uses the same method as Yamauchi et al [2013] where all hot H^+ events in the 4-7 RE were classified. Please refer Yamauchi et al [2013] for the detail of the method and Rème et al. [2001] for the CIS instrument.

Since the hot He^+ event is rare but still have various energy-time morphologies, and since the event takes place in the region where the CIS data are often contaminated by radiation belt particles (we could use only about 300 perigee traversals out of more than 700 traversals with CIS data), we can only take statistics of the occurrence rate, without solid correlation work against any external parameters such as the AE index. With this remark, we classify all He^+ events during 2001-2006 from ion morphology considering the three known energization mechanisms mentioned above. The characteristics of each type of hot He+ events are described in section 2. We then discuss the occurrence rate, their inter-relationship, and the relation with geomagnetic activity in section 3.

2. Cluster Observations

Out of three possible hot He^+ energization mechanisms in the inner magnetosphere mentioned above, we may distinguish only two types of signatures in the CIS data. One is burst-type with no or little energy-time dispersion signatures, indicating that Cluster was located close to the magnetic flux tube in which the local energization took place (Types 1a and 1b). The other is drift type with strong dispersion or even constant energy, indicating a remote source (Types 2a and 2b). On the other hand, we cannot distinguish the hot ions of ionospheric-origin (after some field-aligned acceleration) from trapped ions with very low mirror-altitude (the distinction is given in Yamauchi et al. (1996)), because the loss cone is smaller than the instrument resolution in the surveyed region. For example, the ion zipper [e.g., Fennel et al., 1981; Sheldon and Spence, 1997] could well be mirroring ones [Yamauchi et al, 2013]. In fact, the inner-magnetospheric hot He^+ events with He^+–H^+ differences and with a large field-aligned component do not show any wave activity of field-aligned acceleration type, and therefore, we do not consider such cases. After this classification, we sub-divide into sub-categories by the He^+–H^+ differences or dispersion strength, but these sub-categories are rather morphological.

2.1. Type 1a

Figure 1 shows the CIS/CODIF data from Cluster-4 spacecraft (C4) on 4 May 2004. The hot He^+ with peak differential energy flux of about 150 eV was found at around 07:03–07:06 UT (arrow in Figure 1b), followed by a similar signature with less energy until around 07:07 UT. The intensification is recognized from tens of eV up to as high as 1 keV, mainly in the direction perpendicular to the geomagnetic field as is shown in Figure 1e. The magnetic local time (MLT) is about 20 MLT and the invariant latitude (Ilat) is about -62°.

The H^+ data (Figure 1a) also show a weak intensification at much lower energy (< 35 eV), but otherwise (above 30 eV) the intensity of H^+ is much lower than that of He^+. On the other hand, a weak energy-time (or energy-latitude) dispersed signature extends from the high-energy edge of this H^+ intensification at around 400–700 eV for many tens of minutes, and this stripe is not well recognized in the He^+ data. No O^+ signature (Figure 1c) or He^{++} signature (He^{++} data are not shown here) accompanied it. The absence of He^{++} indicates that the observed He^+ cannot be charge-exchanged He^{++}, which is reasonable for this region because the solar wind cannot directly access there.

The Cluster-1 spacecraft (C1) at a short distance from Cluster-4 also observed a similar signature, while when this signature was observed by Cluster-3 (C3) about half an hour later at a similar location, it was much less distinctive than those in Cluster-1 or Cluster-4. Therefore, this hot He^+ event is temporally and spatially limited. The decay within half an hour suggests that the time scale is less than one hour. However, out of six other similar events, only one event was observed with sufficient (half hour) time lag between two spacecraft, which showed no significant differences. The statistics are too small to conclude anything about the time scale.

2.2. Type 1b

%%%%%% Figure 2 %%%%%%

Figure 2 (3 September 2002) shows a similar event to the one in Figure 1, but with different H^+ and O^+ signatures in different energies and pitch angles. The Cluster-1 data show a sudden enhancement of hot He^+ (mainly < 100 eV) at around 07:58 UT (arrow in Figure 2b). The spacecraft location is about 12 MLT and about –68° Ilat.

This hot He^+ event is accompanied by a hot H^+ enhancement (Figure 2a) in the same energy range (mainly < 100 eV) . However, the intensified hot He^+ have nearly 90° pitch angles as shown in Figure 2e, whereas the intensified hot H^+ have a large field-aligned component (up to 45° pitch angles) as shown in Figure 2d, indicating that the mirror altitude for H^+ is much lower than that for He^+. Furthermore, the peak energy flux density of this hot H^+ enhancement (about $6 \cdot 10^5$ keV cm^{-2} s^{-1} str^{-1} keV^{-1}) is found at a lower energy (less than 35 eV: the lowest energy channel of CODIF) than that of He^+ (about $3 \cdot 10^5$ keV cm^{-2} s^{-1} str^{-1} keV^{-1} at around 70 eV). Furthermore, the hot H^+ population of < 100 eV was not enhanced when the He^+ event took place in Cluster-4 (Figures 2g and 2h) or Cluster-3 (Figures 2m and 2n).

In Figures 2e and 2f, one can also recognize some weak enhancement of low-energy O^+ beyond the noise level slightly after the He^+ enhancement at around 08:01 UT in Cluster-1 (50-200 eV). According to Cluster-4 (Figure 2i) and Cluster-3 (Figure 2o), however, this O^+ enhancement took place when the He^+ signature (Figures 2h and 2n) was weakened and the H^+ signature (Figures 2g and 2m) was enhanced. Furthermore, the characteristic energy of this O^+ signature in Cluster-1 is higher than those of He^+ or even those of the O^+ signature in Cluster-4 or Cluster-3. Only the Cluster-1 signature of the O^+ enhancement might be linked to the He^+ enhancement, but we have no clue to help us answer this question. On the other hand, the pitch angle of this O^+ signature is the same as that of intensified He^+ (about 90 °) in all three spacecraft (Figures 2e, 2k, and 2q).

Unlike the previous example, the 3 September 2002 event lasted so long that both Cluster-4 and Cluster-3 (which traversed the same region after Cluster-4) detected the same signature: at around 08:22 UT (about -70° Ilat) in Cluster-4 and at around 08:42 UT (about -71° Ilat) in Cluster-3. Comparison of data from all three spacecraft also shows that the event location moved outward from ~-68° Ilat to ~-71° Ilat. During 2001–2006, only two similar events are found: in one case the He^+ burst was not observed both half an hour before and half an hour after, whereas in the other case the He^+ event was observed with 1 hour separation at the same magnetic latitude and longitude. Therefore, the event shown in Figure 2 can be a special one that requires a separate study.

Although this He^+ event lasted nearly an hour, which is enough to cause some dispersion at this energy according to both past observations and simulations [Yamauchi et al., 2012, 2014], the energization location is expected to be close to the spacecraft location because there is no energy-time (energy-latitude) dispersion in Figures 2b, 2h, and 2n. Instead, the highest He^+ energy flux density was found at a rather constant energy (around 70 eV) while the intensity decreased during 08:01–08:08 UT in Cluster-1 and 08:23–08:32 UT in Cluster-4.

The observed outward motion of the hot He^+ signature made its location relative to the ion region also outward: Cluster-1 detected the hot He^+ signature several minutes after the decrease of low-energy H^+ (Figures 2a and 2b), while Cluster-4 detected it simultaneously

with the decrease of low-energy H^+ (Figures 2g and 2h). Cluster-3 H^+ data (Figure 2m) is noisy and cannot be used for a comparison.

These decreases of the low-energy H^+ intensity are energy-time (energy-latitude) dispersed, and such dispersion in the noon sector indicates that these low-energy ions are transported by westward ion drift (Ejiri et al., 1980; Ebihara et al., 2001, 2008, Yamauchi et al., 2009b). Therefore, the event is located inside the cavity of these drifting ions (cavity started 07:54 UT in Figure 2a, and 08:22 UT in Figure 2g), and it approaches to the boundary of the westward drifting shell as the time proceeds. Since the drift velocity is the same between different ions at a fixed point and energy, and 25 min is too short for drifting ions to catch up with the ions with the same energy by the slow-down process of drift motion, the change in the relative location from the Cluster-1 observation to the Cluster-4 observation is a puzzle.

The observed He^+ enhancement is located in the outer plasmasphere, according to WHISPER sounder data [Décréau et al., 2001] and EFW data [Gustafsson et al., 2001]. By combining the total electron density measured by the WHISPER instrument and the spacecraft potential measured by the EFW experiment, it is possible to estimate qualitative changes in the plasma density [Pedersen et al., 2001, 2008]. These data (not shown here) indicate that the Cluster-1 plasma density increased from around 07:52 UT toward the perigee, and the Cluster-4 plasma density increased from around 08:00 UT toward the perigee. Embedded in this general trend, plasma density decreased sharply at around 08:19 UT in Cluster-1 and at around 08:38 UT and 08:43 UT in Cluster-4. Therefore, this event could be related to a plasmaspheric plume that is detached from the plasmasphere [e.g., Chappell, 1974; Blanc et al., 1999; Goldstein et al., 2003, 2004; Dandouras et al., 2005; Darrouzet et al., 2008; Pierrard et al., 2008; Lemaire and Pierrard, 2008].

The detachment of the plasmasphere is consistent with the composition change of the hot plasma: after this He^+ event ended at around 08:08 UT in Cluster-1 (Figures 2a-2c) and 08:32 UT in Cluster-4 (Figures 2g-2i); i.e., both the He^+/H^+ ratio and the He^+/O^+ ratio of low-energy ions (< 100 eV) decreased substantially even though the spacecraft was moving inward. Furthermore, He^+ intensity at < 100 eV is enhanced while the intensities of H^+ and O^+ did not change very much after around 08:27 UT (-65° Ilat) in Cluster-1 and 08:45 UT (-66° Ilat) in Cluster-4. This suggests that the present hot He^+ event could well be the cause as well as the result of the plasmasphere detachment.
. On the other hand, a minor intensification of hot He^+ (less intense compared to H^+) with the same pitch-angle and energy characteristics as the main event mentioned above was also observed before 07:48 UT (-70° to -74° Ilat.), i.e., 10 min before the main event started in Cluster-1. This minor event covered a wide region (-70° to -74° Ilat.) where both WHISPER and EFW data show low density (electron density of about 5 cm^{-3}), and is difficult to interpret as the plasmasphere. Unlike the main event inside the detached plasmasphere mentioned above, this minor He^+ enhancement disappeared by the time when Cluster-4 traversed the same region (at around 08:00 UT) where both the electron density (WHISPER) and the low energy proton fluxes (Fig 2b) are enhanced. Cluster-4 detected a minor signature after 08:14 UT (inside of -72° Ilat.), but it is not clear if this is a remnant of what Cluster-1 observed. The difference is not due to a sensitivity difference (this problem might exist for Cluster-3 but

not for Cluster-1 or Cluster-4 in 2002). Thus, the He^+ event disappeared during the plasmasphere expansion (or during the outward motion of the detached plasmasphere).

As mentioned above, the energization location should be close to the spacecraft location. Therefore, we should consider the selective energization mechanism of He^+ as a different mechanism from the plasmasphere detachment even if the hot He^+ event could be related to the detached plasmasphere.

At the inner boundary of the detached plume from the plasmasphere (at 08:19 UT, or -65° Ilat) in Cluster-1, hot ions (both H^+ and He^+, and even O^+) suddenly disappeared in an energy-time (energy-latitude) dispersed manner. Both the plasma density and the hot plasma intensity recovered within a few minutes, but with a stronger energy-time dispersion. The same type of discontinuity is also seen in Cluster-4 at around 08:44 UT (-66° Ilat). The change of the dispersion characteristics indicates that the drift time or distance is longer after this discontinuous boundary than before. It looks like the drift shell between -65° Ilat and -68° Ilat at around 07:58-08:19 UT (Cluster-1) has a slightly faster drift (or corotation) compared to the drift shell between -66° Ilat and -70° Ilat at around 08:22-08:44 UT (Cluster-4).

In Figure 2, we showed an example where H^+ moved in more field-aligned direction than He^+, but the opposite case also exists (2 July 2001; not shown here). The enhanced He^+ flow in the 2 July 2001 event was highly field-aligned whereas the corresponding H^+ at the end of the He^+ event has a peak intensity at 90° pitch angles. Note that it is impossible to judge at the equator whether ions flowing nearly field-aligned [e.g., Fennell et al. 1981; Sheldon and Spence, 1997] are escaping ions from the ionosphere or north-south bouncing ions with a low mirror altitude because no previous instrument, including Cluster, could resolve the loss cone in the equatorial plane [Yamauchi et al., 2013].

2.3. Type 2a

Once the He^+ is energized to more than 100 eV, the magnetic drift (gradient-B drift and curvature drift) causes energy-distance dispersion which is detected as energy-time dispersion in a spacecraft because (1) the drift velocity depends on energy (but not on species, as mentioned in the introduction), and (2) the drift velocity depends on the strength of the magnetic field, i.e., the L value or magnetic shell. Furthermore, ions may be energized adiabatically [Ejiri et al., 1980] if the drift path shifts toward inner shells (lower L-values) experiencing an increase of the magnetic field (this happens particularly for ions drifting from midnight toward the evening sector driven by the E×B drift). In such cases, the ion energy increases to conserve the magnetic moment [Alfvén and Fälthammar, 1963, chapter 2]. For example, cold ions in the nightside can easily be energized to the keV range when the dawn-to-dusk electric field is imposed [Ebihara et al., 2008, Yamauchi et al., 2009b].

%%%%%% Figure 3 %%%%%%

Figure 3 shows one such example on 30 April 2005. The wedge-like energy-time dispersed He^+ (arrow in Figure 3b) are observed starting from < 50 eV at around 08:38 UT to more than 2 keV after 08:54 UT on Cluster-4. The spacecraft location of this He^+ signature is about 21

MLT and inside -62° Ilat (L<4.5). The ion stripes with this dispersion pattern at this local time are most likely westward-drifting ions [Ejiri et al., 1980], and this also applies to He^+.

Similar energy-time dispersed stripes are observed in H^+ five minutes before the He^+ stripe (Figure 3a), and very faintly in 500 eV O^+ at around 08:45 UT (one must examine both the energy-time spectrogram (Figure 3c) and the pitch angle-time spectrogram (Figure 3f) to recognize it but the signature is beyond the noise level), but neither was simultaneously observed at the same energy as He^+. The pitch angles are nearly 90° for all stripes.

Since the ion drift is mass-independent, i.e., ions with the same initial energy experience the same energization for different species during the drift, He^+ should somewhat have been filtered from H^+ and O^+ at the location where He^+ started to drift, probably in the similar manner as those shown in Figures 1 and 2.

One possibility is that He^+ was filtered already at the starting location of the drift. If such filtering occurs, we should also be able to observe energy-time dispersed He^+ stripes without any similar H^+ stripes at any nearby time as an extreme case. One such hot He^+ event can be the event observed on 2 July 2005 (not shown here). However, this could also be due to its location: it was observed over the perigee, and if the H^+ signature is located at a lower altitude than the He^+ signature, Cluster cannot detect it. Therefore, we could not use the 2 July 2005 as proof of the filtering.

2.4. Type 2b

%%%%%% Figure 4 %%%%%%

Finally, Figure 4 shows an example of the hot drifting He^+ that is accompanied by the hot drifting O^+ without a clear H^+ signature (19 March, 2001). Because the observation was during the earliest part of the Cluster mission, the micro-channel-plate (MCP) was quite sensitive (lowest one-count level) and we could detect relatively faint signatures rather clearly. In other words, it is difficult to detect a similar event in the later part of the mission (we could detect it only during the first 13 months of CIS observations).

In Figure 4b one can recognize a band of enhanced He^+ at a narrow energy range around 1 keV over one hour (marked by the arrow), starting from the wedge-like energy-time (energy-latitude) dispersed signature at around 09:11 UT in Cluster-4. The spacecraft location of this He^+ signature is about 23 MLT and inside ±62° Ilat. The other spacecraft (Cluster-1 at 5 min before and Cluster-3 at 3 min before) observed the same signature at about the same location.

During the entire period of this He^+ band (09:10–10:16 UT), the H^+ signature at the same energy range (Figure 4a) is seen faintly and only partially (e.g., 09:10–09:30 UT) at about the noise level during the rest of the time. The O^+ signature (Figure 4c) is clearer than the H^+ signature but not as intense as He^+ signature. The O^+ band is found at the energy level where He^+ fluxes are less intense than the neighboring energy range. Therefore, the O^+ signature cannot be contamination from He^+. The result indicates that both He^+ (mass/charge ratio of 4) and O^+ (mass/charge ratio of 16) were filtered out from H^+ at the same starting location, in different ways and at different energies in terms of mass per charge.

3. Summary and Discussion

Since the energization of only He^+ (without sufficient H^+ population that can provide energy to He^+ cyclotron wave) has not been reported over more than 40 years of inner magnetospheric studies [e.g., Geiss et al., 1979; Young et al., 1982; Lennartsson and Sharp, 1982; Collin et al., 1988; Fuselier and Anderson, 1996; Blanc et al., 1999; Mouikis et al., 2002; Peterson et al., 2008], any interpretation might introduce a misleading prejudice. Even our morphological classification has the same risk. With this concern in mind, we summarize and discuss the results.

Table 1 summarizes the hot He^+ events that are not accompanied by the same type H^+ signature (H^+ flux is very low, pitch angles are completely different, or characteristic energy is different) during 2001–2006 as observed by Cluster-4 with the CIS/CODIF instrument. Out of about 300 perigee traversals with moderate or less contamination from radiation belt particles, such that CIS can detect hot He^+ events, we found 20 clear examples of hot He^+ events beyond the noise level and nearly 10 unclear examples (intensity is low, He^+/O^+ ratio is not very high, or difficult to judge the instrumental effect).

Figure 5 shows the probability of observing hot He^+ events (all types are added) at different quadrants. Since the CIS instrument was significantly contaminated by the radiation belt particles during 2003 (this also caused significant degradation of the MCP and resultant changes in the one-count level [Kistler et al., 2013]), the occurrence rate in the noon and night sector dropped sharply. Such a decrease is also observed for H^+ events [Yamauchi et al., 2013]. On the other hand, the increase of the dusk sector probability is substantial, i.e., the declining phase of the solar cycle increases the probability of hot He^+ events.

We classified these He^+ events into two categories based on possible mechanism (see introduction) and two subcategories each from the morphology in the spectrogram, respectively:
Type 1: Short intensification of He^+ (1a) without corresponding H^+ or O^+ signatures, or at least (1b) with H^+ signature at different pitch angles.
Type 2: Energy-latitude dispersed He^+ stripe that continues for tens of minutes at a hundreds to a few thousand eV range (2a) at different drift shell from energy-latitude dispersed H^+ stripes, or (2b) with very weak H^+ signature if the energy is nearly constant.

Note that no single event has exactly the same morphology as the other events, and even the local time scatters within each category (Type 1a and 2a without clear H^+ signature or O^+ signature is found somewhat in the dust sector, though). Since each category includes so few events, and the MCP significantly degraded during the 6 years of observations, it is also difficult to classify the event based solidly on physical processes. Therefore, solid classification is also a future task, e.g., by combining the Van Allen Probe data and drift simulations.

Table 1 also includes geomagnetic activities during and before the hot He^+ events. Type 1a might be related to on-going or very recent magnetospheric activities, and Type 2b might be related to quiet periods that allow undisturbed drift. From the past statistical and simulation

results of low-energy H^+, Type 2 are expected to be related to past substorm activities [Ebihara et al., 2008; Yamauchi et al., 2009b, 2013]. On the other hand, we still have examples of extremely long quiet cases in these categories (21 August 2001 and 21 September 2001), which are located at near noon.

The quiet conditions for noon events are also found in Type 1b. Such hot He^+ must have been energized locally before the ion drift forms dispersion. Except for these noon events, Type 1 He^+ burst events without energy-time dispersion (which are located in the dusk-to-night sector) are somewhat related to substorm activities. This in turn suggests that Type 2 He^+ events must be traced back by the drift simulation to understand the selective energization of He^+ or filtering mechanisms from H^+ and O^+.

Yamauchi et al. [2012] reported that about one third of the equatorially-trapped warm ions [e.g., Olsen et al., 1987; Blanc et al., 1999] include the He^+ signature at higher energies than H^+. However, the equatorially-trapped warm ions are found at all MLT and all geomagnetic conditions. Furthermore, the present observations are not confined within the equator but are found also at some distance from the equator, and the pitch angle distributions are quite different between He^+ and H^+, when H^+ is simultaneously observed (i.e., Type 1b). Therefore, the present events and the equatorially-trapped warm ions are not directly related to each other, although the mass-dependent energization mechanism might have some common basis.

According to the satellite potential and plasma frequency measurement, the peak energy flux for the detected hot He^+ was located within the outer plasmasphere for all examples. We searched the region between 4-7 R_E, which includes the region outside the plasmapause, and therefore, the outer plasmaspheric location is not due to the search criterion. This result indicates that the plasmaspheric cold He^+ is most likely the ultimate source.

Finally the Van Allen Probe recently found He^+ enhancement [J.M. Jahn, presentation at 23rd Cluster workshop, 2013]. It would be useful to compare the characteristics of hot He^+ events between the Cluster observations (polar orbit) and the Van Allen Probe (equatorial orbit) observations because all satellites cover different regions of the inner magnetosphere.

4. Conclusions

Using Cluster spacecraft-4 CIS/CODIF data during the 2001–2006 period that have about 300 north-south symmetric perigee traversals over the inner magnetosphere covering L>4 with valid He^+ measurements, we found 20 clear examples and nearly 10 unclear examples of hot He^+ enhancement at the 0.03-1 keV range, without the same types of hot H^+ at the same energy. These He^+ events are quite unexpected because drift theory predicts the same energization and the same drift velocity between different species if the initial energy is the same. Since the He^+/H^+ ratio of cold ions in the plasmasphere is always less than unity [e.g., Young et al., 1982; Dandouras, 2013], we need a filtering mechanism that selects only cold He^+ and separates them from H^+ and O^+.

From the morphology in the spectrograms, shown in Figures 1-4, these hot He^+ events are classified into 2 types: burst type and drifting type. Correlation with the geomagnetic activity

indicates that the short intensification of He^+ without corresponding H^+ in the evening-night sector is observed during or right after a substorm activity, suggesting that the plasmasphere might be energized in a mass dependent way in the evening sector during substorms.

On the contrary, the selective He^+ energization can also take place during quiet periods near noon. Also, enhanced He^+ that continues for tens of minutes without corresponding H^+ are found after long quiet times, i.e., after long drift, and therefore the source of these He^+ must be remote from the observation point. Numerical simulations will be at least in the future needed to estimate the location and the geomagnetic conditions at the time of the He^+ filtering.

Acknowledgements
The AE index from 11 stations is provided by WDC-C2 for geomagnetism at Kyoto University. The Cluster project is managed by the European Space Agency (ESA). The EFW data and WHISPER data, used in our analyses, are provided by M. Andre and P. Decreau through the Cluster Active Archive (CAA). This work is partly supported by the Swedish National Space Board. Yamauchi thanks programmes for disabled people in Sweden, which have made it possible for him to work.

References

Alfvén, H. and C. G. Fälthammar (1963), Cosmical Electrodynamics, Fundamental Principles, Clarendon Press, Oxford.

Blanc, M., J.L. Horwitz, J.B. Blake, I. Daglis, J.F. Lemaire, M.B. Moldwin, S. Orsini, R.M. Thorne, and R.A. Wolfe (1999), Source and loss processes in the inner magnetosphere, Space Sci. Rev., 88(1-2), 137-206, doi:10.1023/A:100520381735.

Burch, J. L., S. B. Mende, D. G. Mitchell, T. E. Moore, C. J. Pollock, B. W. Reinisch, B. R. Sandel, S. A. Fuselier, D. L. Gallagher, J. L. Green, J. D. Perez, and P. H. Reiff (2001), Views of Earth's magnetosphere with the IMAGE satellite, Science, 291(5504), 619-624, doi:10.1126/science.291.5504.619.

Burch, J. L. (2005), Magnetospheric imaging: Promise to reality, Rev. Geophys., 43(3), doi:10.1029/2004RG000160.

Chappell, C. R. (1974), Detached plasma regions in the magnetosphere. J. Geophys. Res., 79(13), 1861–1870, doi:10.1029/JA079i013p01861.

Collin, H. L., W. K. Peterson, J. F. Drake, and A. W. Yau (1988), The helium components of energetic terrestrial ion upflows: Their occurrence, morphology, and intensity, J. Geophys. Res., 93, 7558--7564, doi:10.1029/JA093iA07p07558.

Dandouras, I. (2013), Detection of a plasmaspheric wind in the Earth's magnetosphere by the Cluster spacecraft, Ann. Geophys., 31, 1143-1153, doi:10.5194/angeo-31-1143-2013.

Dandouras, I., V. Pierrard, J. Goldstein, C. Vallat, G. K. Parks, H. Rme, C. Gouillart, F. Sevestre, M. McCarthy, L. M. Kistler, B. Klecker, A. Korth, M. B. Bavassano-Cattaneo, P. Escoubet, and A. Masson (2005), Multipoint observations of ionic structures in the plasmasphere by CLUSTER–CIS and comparisons with IMAGE-EUV observations and with model simulations, in Inner Magnetosphere Interactions: New Perspectives From Imaging, Geophys. Monogr. Ser., vol. 159, edited by J. Burch, M. Schulz, and H. Spence, 23–53, AGU, Washington, D. C., doi:10.1029/159GM03.

Darrouzet, F., J. De Keyser, P. M. E. Décréau, F. El Lemdani-Mazouz, and X. Vallières (2008), Statistical analysis of plasmaspheric plumes with Cluster/WHISPER observation, Ann. Geophys., 26, 2403-2417, doi:10.5194/angeo-26-2403-2008.

Darrouzet, F., D. L. Gallagher, N. André, D. L. Carpenter, I. Dandouras, P. M. E. Décréau, J. De Keyser, R. E. Denton, J. C. Foster, J. Goldstein, M. B. Moldwin, B. W. Reinisch, B. R. Sandel, and J. Tu (2009a), Plasmaspheric density structures and dynamics: Properties observed by the CLUSTER and IMAGE missions, Space Sci. Rev., 145(1-2), 55-106, doi:10.1007/s11214-008-9438-9.

Darrouzet, F., J. De Keyser, and V. Pierrard (Eds.) (2009b), The Earth's Plasmasphere: A CLUSTER and IMAGE Perspective, 296 pp., Springer Science+Business Media, BV, doi:10.1007/978-1-4419-1323-4, ISBN-978-1-4419-1322-7, e-ISBN-978-1-4419-1323-4.

Décréau, P. M. E., Fergeau, P., Krasnoselskikh, V., Le Guirriec, E., Lévêque, M., Martin, P., Randriamboarison, O., Rauch, J. L., Sené, F. X., Séran, H. C., Trotignon, J. G., Canu, P., Cornilleau, N., de Féraudy, H., Alleyne, H., Yearby, K., Mögensen, P. B., Gustafsson, G., André, M., Gurnett, D. C., Darrouzet, F., Lemaire, J., Harvey, C. C, Travnicek, P., and et al. (2001), Whisper Experimenters Group: Early results from the Whisper instrument on Cluster: an overview, Ann. Geophys., 19, 1241-1258, doi: 10.5194/angeo-19-1241-2001.

Denton, M. H., G. J. Bailey, C. R. Wilford, A. S. Rodger, and S. Venkatraman (2002), He+ dominance in the plasmasphere during geomagnetically disturbed periods: 1. Observational results, Ann. Geophys., 20, 461-470, doi:10.5194/angeo-20-461-2002.

Ebihara, Y., M. Yamauchi, H. Nilsson, R. Lundin, and M. Ejiri (2001), Wedge-like dispersion of sub-keV ions in the dayside magnetosphere: Particle simulation and Viking observation, J. Geophys. Res., 106, 29571–29584, doi:10.1029/2000JA000227.

Ebihara, Y., L. M. Kistler, and L. Eliasson (2008), Imaging cold ions in the plasma sheet from the Equator-S satellite, Geophys. Res. Lett., 35, L15103, doi:10.1029/2008GL034357.

Ejiri, M., R. A. Hoffman, and P. H. Smith (1980), Energetic particle penetration into the inner magnetosphere, J. Geophys. Res., 85(A2), 653–663, doi:10.1029/JA085iA02p00653

Escoubet, C. P., C. T. Russell, and R. Schmidt (Eds.) (1997), The Cluster and Phoenix Missions, 658 pp., Kluwer Academic Publishers, Dordrecht.

Escoubet, C. P., M. Fehringer, M., and M. Goldstein: The Cluster mission, Ann. Geophys., 19, 1197-1200, doi:10.5194/angeo-19-1197-2001, 2001.

Fennell, J. F., D. R. Croley Jr., and S. M. Kaye (1981), : Low-energy ion pitch angle distributions in the outer magnetosphere: Ion zipper distributions, J. Geophys. Res., 86, 3375--3382, doi:10.1029/JA086iA05p03375.

Fuselier, S. A., and B. J. Anderson (1996), Low energy He+ and H+ distributions and proton cyclotron waves in the afternoon equatorial magnetosphere, J. Geophys. Res., 101, 13255-13265, DOI: 10.1029/96JA00292.

Geiss, J., H. Balsiger, P. Eberhardt, H. P. Walker, L. Weber, D. T. Young, and H. Rosenbauer (1979), Dynamics of magnetospheric ion composition as observed by the GEOS mass spectrometer, In Advances in Magnetosperic Physics with GEOS-1 and ISEE, Springer Netherlands, p. 217-246.

Goldstein, J., B. R. Sandel, M. R. Hairston, and P. H. Reiff (2003), Control of plasmaspheric dynamics by both convection and sub-auroral polarization stream, Geophys. Res. Lett., 30(24), 2243, doi: 10.1029/2003GL018390.

Goldstein, J., B. R. Sandel, M. F. Thomsen, M. Spasojevic, and P. H. Reiff (2004), Simultaneous remote sensing and in situ observations of plasmaspheric drainage plumes, J. Geophys. Res., 109, A03202, doi:10.1029/2003JA010281.

Gustafsson, G., M. André, T. Carozzi, A. I. Eriksson, C.-G. Fälthammar, et al. (2001), First results of electric field and density observations by Cluster EFW based on initial months of operation, Ann. Geophys., 19, 1219-1240, doi:10.5194/angeo-19-1219-2001.

Horne, R. B., and R. M. Thorne (1997), Wave heating of He+ by electromagnetic ion cyclotron waves in the magnetosphere: Heating near the H+-He+ bi-ion resonance frequency, J. Geophys. Res., 102, 11457--11471, doi:10.1029/97JA00749.

Johnson, R. G., D. Sharp, and G. Shelley (1974), The discovery of energetic He+ ions in the magnetosphere, J. Geophys. Res., 79, 3135--3139, doi:10.1029/JA079i022p03135.

Kistler, L. M., C. G. Mouikis, and K. J. Genestreti, (2013), In-flight Calibration of the Cluster/CODIF sensor, Geosci. Instrum. Method. Data Syst., 2, 225–235, doi:10.5194/gi-2-225-2013.

Lemaire, J. F., and V. Pierrard (2008), Comparison between two theoretical mechanisms for the formation of the plasmapause and relevant observations. Geomagnetism and Aeronomy, 48(5), 553-570, doi:10.1134/S0016793208050010.

Lennartsson, W., and R. D. Sharp (1982), A comparison of the 0.1–17 keV/e ion composition in the near equatorial magnetosphere between quiet and disturbed conditions, J. Geophys. Res., 87, 6106--6120, doi:10.1029/JA087iA08p06109

Lund, E. J., E. Mobius, L. Tang, L. M. Kistler, M. A. Popecki, D. M. Klumpar, W. K. Peterson, E. G. Shelley, B. Klecker, D. Hovestadt, M. Temerin, R. E. Ergun, J. P. McFadden, C. W. Carlson, F. S. Mozer, R. C. Elphic, R. J. Strangeway, C. A. Cattell, R. F. Pfaff (1998), FAST observations of preferentially accelerated He+ in association with auroral electromagnetic ion cyclotron waves, Geophys. Res. Lett., 12, 2049-2052, doi:10.1029/98GL00304.

Mouikis, C. G., L. M. Kistler, W. Baumjohann, E. J. Lund, A. Korth, B. Klecker, E. Mobius, M. A. Popecki, J. A. Sauvaud, H. Rème, A. M. Di Lellis, M. McCarthy, and C. W. Carlson (2002), Equator-S observations of He+ energization by EMIC waves in the dawnside equatorial magnetosphere, Geophys. Res. Lett., 29(10), doi:10.1029/2001GL013899.

Nakamura, N., I. Yoshikawa, A. Yamazaki, K. Shiomi, Y. Takizawa, M. Hirahara, K. Yamashita, Y. Saito and W. Miyake (2000), Terrestrial plasmaspheric imaging by an extreme ultraviolet scanner on planet-B, Geophys. Res. Lett., 27(2), 141–144, doi:10.1029/1999GL010732.

Olsen, R. C., S. D. Shawhan, D. L. Gallagher, J. L. Green, C. R. Chappell, and R. R. Anderson (1987), Plasma observations at the Earth's magnetic equator, J. Geophys. Res., 92(A3), 2385–2407, doi:10.1029/JA092iA03p02385.

Pedersen, A., P. Décréau, C.-P. Escoubet, G. Gustafsson, H. Laakso, P.-A. Lindqvist, B. Lybekk, A. Masson, F. Mozer, and A. Vaivads (2001), Four-point high time resolution information on electron densities by the electric field experiments (EFW) on Cluster, Ann. Geophys., 19, 1483-1489, doi:10.5194/angeo-19-1483-2001.

Pedersen, A., B. Lybekk, M. André, A. Eriksson, A. Masson, et al. (2008), Electron density estimations derived from spacecraft potential measurements on Cluster in tenuous plasma regions, J. Geophys. Res., 113, A07S33, doi:10.1029/2007JA012636.

Peterson, W. K., L. Andersson, B. C. Callahan, H. L. Collin, J. D. Scudder, and A. W. Yau (2008), Solar-minimum quiet time ion energization and outflow in dynamic boundary related coordinates, J. Geophys. Res., 113, A07222, doi:10.1029/2008JA013059.

Pierrard, V., G. V. Khazanov, J. Cabrera, and J. Lemaire (2008), Influence of the convection electric field models on predicted plasmapause positions during magnetic storms, J. Geophys. Res., 113, A08212, doi:10.1029/2007JA012612.

Rème, H., C. Aoustin, J. M. Bosqued, I. Dandouras, B. Lavraud, J. A. Sauvaud, A. Barthe, J. Bouyssou, Th. Camus, O. Coeur-Joly, A. Cros, J. Cuvilo, F. Ducay, Y. Garbarowitz, J. L. Medale, E. Penou, H. Perrier, D. Romefort, J. Rouzaud, C. Vallat, D. Alcaydé, C. Jacquey, C. Mazelle, C. d'Uston, E. Möbius, L. M. Kistler, K. Crocker, M. Granoff, C. Mouikis, M. Popecki, M. Vosbury, B. Klecker, D. Hovestadt, H. Kucharek, E. Kuenneth, G. Paschmann, M. Scholer, N. Sckopke, E. Seidenschwang, C. W. Carlson, D. W. Curtis, C. Ingraham, R. P. Lin, J. P. McFadden, G. K. Parks, T. Phan, V. Formisano, E. Amata, M. B. Bavassano-Cattaneo, P. Baldetti, R. Bruno, G. Chionchio, A. Di Lellis, M. F. Marcucci, G. Pallocchia, A. Korth, P. W. Daly, B. Graeve, H. Rosenbauer, V. Vasyliunas, M. Mccarthy, M. Wilber, L. Eliasson, R. Lundin, S. Olsen, E. G. Shelley, S. Fuselier, A. G. Ghielmetti, W. Lennartsson, C. P. Escoubet, H. Balsiger, R. Friedel, J.-B. Cao, R. A. Kovrazhkin, I. Papamastorakis, R. Pellat, J. Scudder, B. Sonnerup (2001), First multispacecraft ion measurements in and near the Earth's magnetosphere with the identical Cluster ion spectrometry (CIS) experiment, Ann. Geophys., 19, 1303–1354, doi:10.5194/angeo-19-1303-2001.

Roeder, J. L., J. F. Fennell, M. W. Chen, M. Schulz, M. Grande, and S. Livi (1996), CRRES observations of the composition of the ring-current ion populations, Adv. Space Res., 17, 17--24, doi:10.1016/0273-1177(95)00689-C.

Roederer, J.G. (1970), Dynamics of Geomagnetically Trapped Radiation, Physics and Chemistry in Space, 2, Springer-Verlag Berlin Heidelberg, New York, doi:10.1007/978-3-624-49300-3.

Sandel, B. R., A. L. Broadfoot, C. C. Curtis, R. A. King, T. C. Stone, R. H. Hill, J. Chen, O. H. W. Siegmund, R. Raffanti, D. D. Allred, R. Steven Turley, and D. L. Gallagher (2000), The Extreme Ultraviolet Imager Investigation for the IMAGE Mission, Space Sci. Rev., 91, 197-242, doi:10.1023/A:1005263510820.

Sandel, B. R., J. Goldstein, D. L. Gallagher, and M. Spasojević (2003), Extreme ultraviolet imager observations of the structure and dynamics of the plasmasphere, Space Sci. Rev., 109, 25-46, doi:10.1023/B:SPAC.0000007511.47727.5b.

Sheldon, R. B. and H. E. Spence (1997), Alfvén boundaries: Noses and zippers, Adv. Space Res., 20, 445–448, doi:10.1016/S0273-1177(97)00501-2.

Williams, D. J., E. C. Roelof, and D. G. Mitchell (1992), Global Magnetospheric Imaging, Rev. Geophys., 30(3), 183-208, doi:10.1029/92RG00732.

Yamauchi, M., R. Lundin, L. Eliasson, and O. Norberg (1996), Meso-scale structures of radiation belt/ring current detected by low-energy ions, Adv. Space Res., 17(2), 171–174, doi:10.1016/S0273-1177(95)00531-1.

Yamauchi, M., I. Dandouras, P. W. Daly, G. Stenberg, H. U. Frey, P.-A. Lindqvist, Y. Ebihara, H. Nilsson, L. Lundin, H. Rème, M. Andréé, E. A. Kronberg, A. Balogh and M. Henderson (2009a), Magnetospheric solitary structure maintained by 3000 km/s ions as a cause of westward moving auroral bulge at 19 MLT, Ann. Geophys., 27, 2947–2969, doi:10.5194/angeo-27-2947-2009.

Yamauchi, M., Y. Ebihara, I. Dandouras, and H, Rème (2009b), Dual source populations of substorm-associated ring current ions, Ann. Geophys., 27, 1431–1438, doi:10.5194/angeo-27-1431-2009.

Yamauchi, M., I. Dandouras, H. Rème and F. El-Lemdani Mazouz (2012), Equatorially confined warm trapped ions at around 100 eV near the plasmapause, Geophys. Res. Lett., 39, L15101, doi:10.1029/2012GL052366.

Yamauchi, M., I. Dandouras, H. Rèeme, R. Lundin and L. M. Kistler (2013), Cluster observation of few-hour scale evolution of structured plasma in the inner magnetosphere, Ann. Geophys., 31, 1569–1578, doi:10.5194/angeo-31-1569-2013.

Yamauchi, M., Y. Ebihara, H. Nilsson and I. Dandouras (2014), Ion drift simulation of sudden appearance of sub-keV structured ions in the inner magnetosphere, Ann. Geophys., 32, 83-90, doi:10.5194/angeo-32-83-2014.

Yoshikawa, I., A. Yamazaki, K. Shiomi, K. Yamashita, Y. Takizawa, and M. Nakamura (2000), Photometric measurement of cold helium ions in the magnetotail by an EUV scanner onboard Planet-B: Evidence of the existence of cold plasmas in the near-Earth plasma sheet, Geophys. Res. Lett., 27(21), 3567-3570, doi:10.1029/2000GL00010.

Young, D.T., S. Perraut, A. Roux, C. de Villedary, R. Gendrin, A. Korth, G. Kremser, and D. Jones (1981), Wave-particle interactions near Ω_{He+} observed on GEOS 1 and 2, 1. Propagation of ion cyclotron waves in He^{+}-rich plasma, J. Geophys. Res., 86(A8), 6755--6772, doi:10.1029/JA086iA08p06755.

Young, D.T., H. Balsiger and J. Geiss (1982), Correlations of magnetospheric ion composition with geomagnetic and solar activity, J. Geophys. Res., 87(A11), 9077–9096, doi:10.1029/JA087iA11p09077.

Table 1: Cluster CIS observations of hot He^+ ion events

date (C4)	UT*1	MLT	Ilat (°)	R*2	type	C1*1,3	C3*1,3	previous AL	AL value
2002-03-30	08:17	22	+61	4.4	1a	08:16	08:18	**200 nT@0.5h**	**onset@0h**
2003-05-30	06:25	19	+59	3.9	1a/2a?	without	n/a	**600 nT@5h**	100 nT
2003-08-12	01:24	14	-65	4.8	1a	n/a	n/a	**substorm**	500 nT
2003-11-22	08:44	8	+64	4.3	1a/2a?	08:43	08:44	**substorm**	50 nT
2004-05-04	07:03	21	-62	4.4	1a	07:05	07:35	**300 nT@3h**	150 nT
2005-05-28	20:10	19	-60	4.2	1a	n/a	20:43	**substorm**	700 nT
2005-07-02	02:26	17	63	5.0	1a/2b?	n/a	02:12	**substorm**	200 nT
2001-09-18	15:40	11	+64	4.1	1b	without	without	quiet=8h	quiet
2002-09-03	08:22	12	-69	4.9	1b	07:58	08:42	quiet>10h	quiet
2006-05-05	00:06	21	-62	4.8	1b/2a?	n/a	23:07	**onset@0.5h**	150 nT
2001-06-20	04:26	17	-61	4.1	2a	04:29	without	quiet=2h	**onset@0h**
2001-08-21	00:53	13	-65	4.3	2a	00:48	01:27	quiet=6h	quiet
2005-04-30	08:40	21	-61	4.2	2a	n/a	08:53	**substorm**	150 nT
2005-06-05	00:06	19	-63	5.1	2a	n/a	n/a	**substorm**	400 nT
2001-03-16	23:54	23	62	4.0	2b	23:50	23:51	quiet=3h	quiet
2001-03-19	09:17	23	59-61	4.0-4.1	2b	09:11	09:13	quiet=1h	quiet
2001-07-02	02:14	16	60	4.0	2b	02:15	02:24	50 nT=3h	onset@0h
2001-09-21	00:21	11	-61	4.2	2b/2a?	00:24	00:59	quiet=1h	quiet
2001-12-15	16:29	5	-60	4.2	2b	16:36	n/a	quiet=2h	quiet
2002-02-22	15:46	0	60-61	4.4	2b	n/a	n/a	quiet=1h	quiet

*1: start of the main event

*2: geocentric distance (R_E)

*3: "without" means that no signature is detected; "n/a" means that data is missing, highly contaminated, or noisy such that we cannot judge.

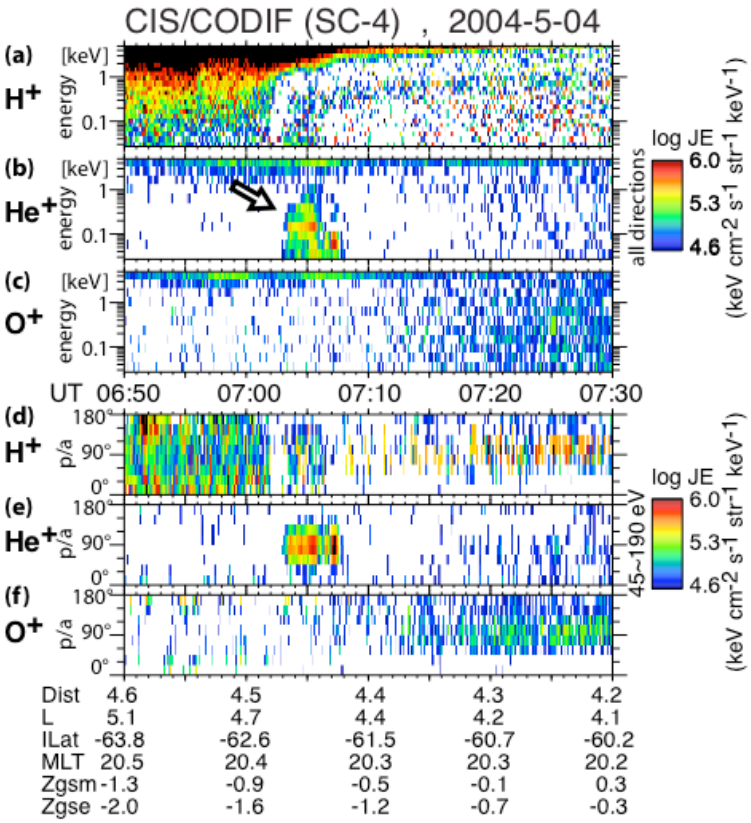

Figure 1: (a-c) Energy–time and (d-f) pitch angle–time spectrograms of differential energy fluxes (keV cm-2 s-1 str-1 keV-1) for protons (H^+), single-charged helium ions (He^+), and oxygen ions (O^+) observed by CIS/CODIF on board Cluster-4 during perigee traversal on 4 May 2004. Note that the lowest limit of CODIF is 30 eV during normal operation.

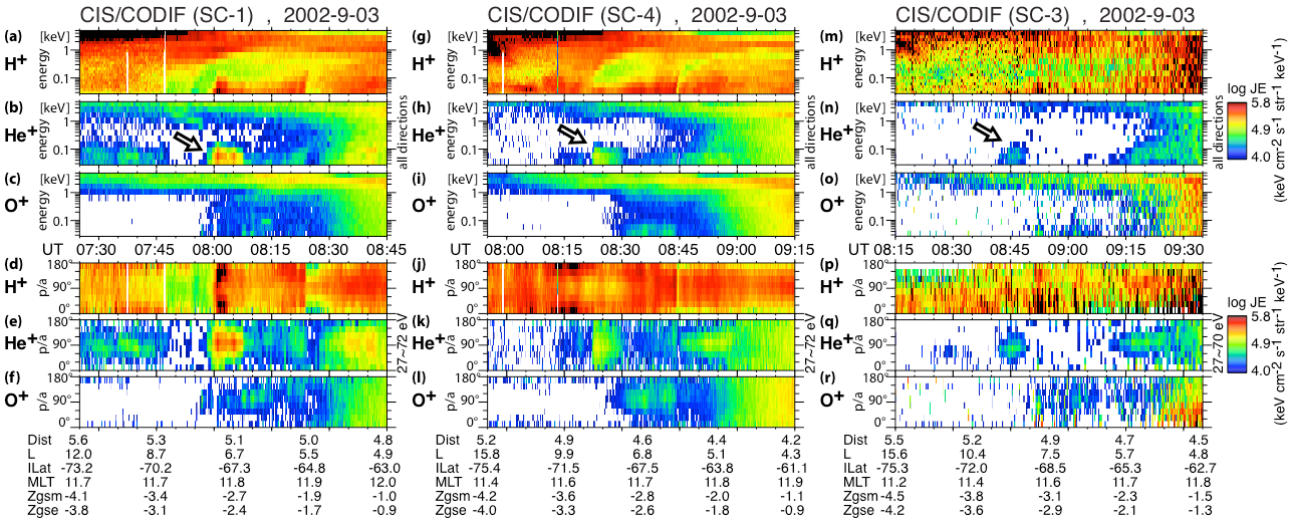

Figure 2: The same format as Figure 1 for 3 September 2002 event for all spacecraft: (a-f) Cluster-1, (g-l) Cluster-4, and (m-r) Cluster-3.

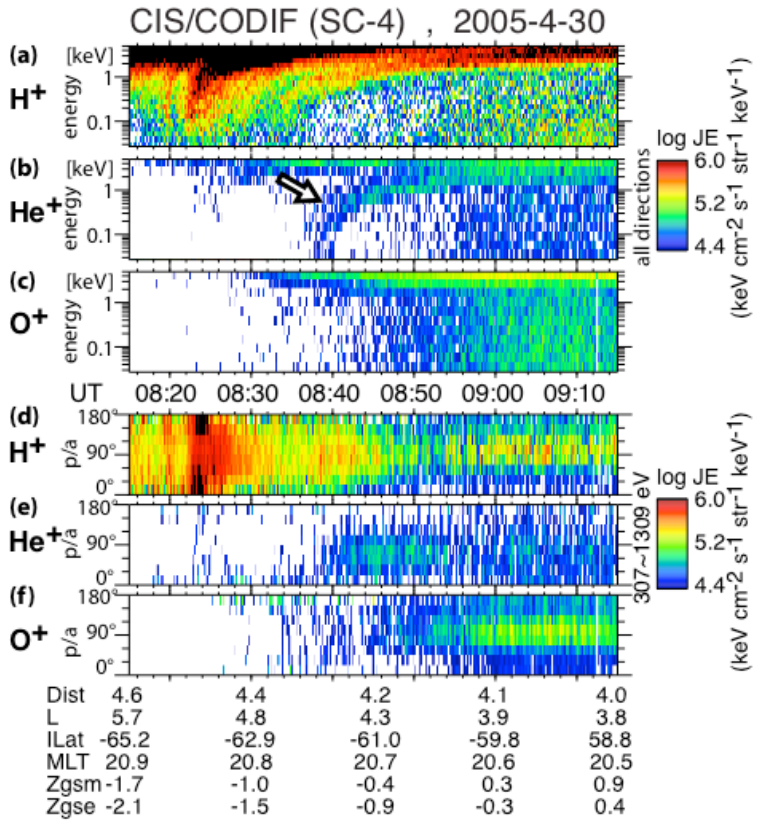

Figure 3: The same format as Figure 1 for the 30 April 2005 event for Cluster-4.

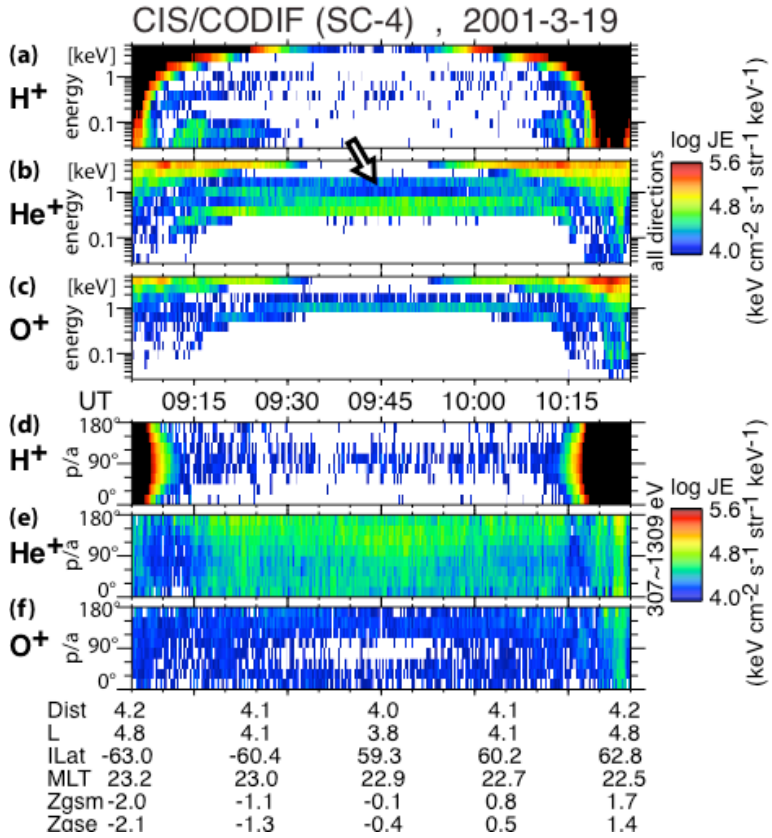

Figure 4: The same format as Figure 1 for the 19 March 2001 event for Cluster-4.

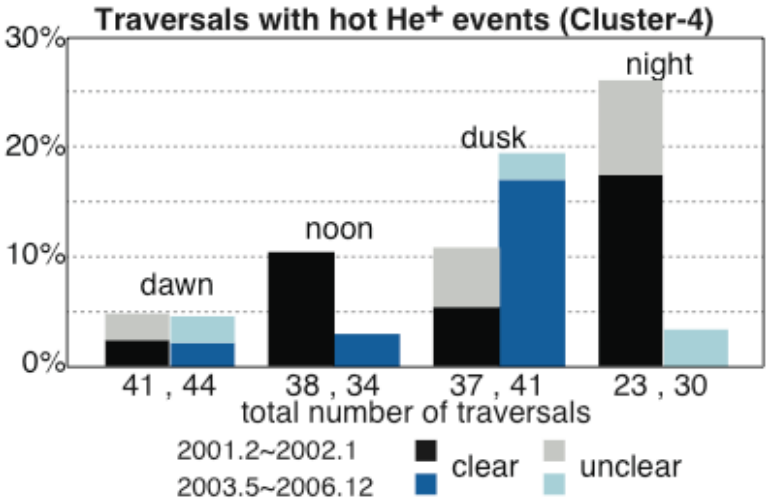

Figure 5: Probabilities of detecting the hot He^{+} events during a perigee traversal (all types of Table 1 are added) by Cluster-4 CIS/CODIF instrument. Since Cluster orbit is synchronous to the solar system, sectors are defined as dusk when Cluster traversed the equator during 16 April - 15 July, noon during 16 July - 15 October, dawn during 16 October - 15 January, and night during 16 January - 15 April. The unclear cases are observations that we could not judge. To elucidate the degradation effect of the sensor, data are divided into Feb 2001 – Jan 2003 and May 2003 – Dec 2006 (no data during Feb–Apr 2003 was clean from contamination by the radiation belt particles). Number at the bottom of each bar is the total number of traversals in each sector.